Available online at www.sciencedirect.com

ScienceDirect

Journal of Molecular Catalysis A: Chemical 281 (2008) 35–43

JOURNAL OF MOLECULAR CATALYSIS A: CHEMICAL

www.elsevier.com/locate/molcata

Mechanistic details of atomic layer deposition (ALD) processes for metal nitride film growth

Hugo Tiznado, Menno Bouman, Byung-Chang Kang, Ilkeun Lee, Francisco Zaera *

Department of Chemistry, University of California, Riverside, CA 92521-0403, USA

Available online 19 June 2007

Abstract

The reaction mechanism of atomic layer deposition (ALD) processes for the deposition of metal nitrides has been characterized by a combination of surface-sensitive techniques, X-ray photoelectron (XPS) and infrared (IR) spectroscopies in particular. The growth of titanium nitride films using alternate doses of $TiCl_4$ and NH_3 is discussed first. It was found that exposure of the surface to the first reactant ($TiCl_4$) is accompanied by the partial loss of chlorine atoms and the reduction of the Ti atoms, and that a subsequent ammonia treatment removes most of the remaining chlorine and leads to the formation of a nitride. Both half-reactions were proven self-limited, and repeated ALD cycles were shown to lead to the buildup of thick films, as desired. However, it was found that the grown films consist of a Ti_3N_4 layer on top of the expected TiN, suggesting that the reduction of the Ti^{4+} species may occur during the $TiCl_4$, not NH_3, dosing step. This conclusion seems to be general, since similar behavior was observed for the deposition of tantalum and zirconium nitrides using $TaCl_5$ and $Zr[N(C_2H_5)(CH_3)]_4$, respectively.
© 2007 Elsevier B.V. All rights reserved.

Keywords: Atomic layer deposition (ALD); Thin films; Metal nitrides; XPS; Infrared spectroscopy

1. Introduction

Conformal coatings, that is, thin films that closely follow the shape of the underlying structures they cover, are a crucial component in a wide variety of modern technologies, including those involving optical and optoelectronic elements [1–5], magnetic storage devices [6,7], tribological, heat and corrosion barriers [8–10], biocompatible protheses [11], membranes, [12,13] and catalysts [14–17]. In microelectronics in particular, most manufacturing processes require the deposition of films of insulators or conductors and the growth of diffusion, adhesion, and protection barriers for the in situ buildup of capacitors, metal interconnects, diodes, transistors, and other elements within integrated circuits [18–20]. The deposition methods available for the growth of such thin films can be broadly divided into physical and chemical in nature: physical vapor deposition (PVD) methods include sputtering, evaporation, and sublimation [21], whereas chemical vapor deposition (CVD) processes are based on the adsorption and chemical conversion of molecular precursors on the surface [19,20]. Both PVD and CVD have found important uses in industry, but CVD processes have been gaining ground in modern times because of their ability to produce smooth and homogeneous conformal films on surfaces with complex topographies [22]. Modern electronic devices are now routinely prepared with sub-100 nm individual structures of very high aspect ratios and many narrow and deep holes and trenches [23,24], and most physical deposition methods are intrinsically directional and therefore ill suited for such applications. Chemical-based processes, on the other hand, are isotropic and can better handle film deposition on rough surfaces.

Various CVD methods have been developed over the years to address specific needs in different applications [25]. Among the advantages of CVD, the following are often cited:

- Their ability to produce highly dense and pure materials and uniform films with good reproducibility and adhesion;
- Their capacity to control crystal structure, surface morphology, and orientation by controlling the CVD process parameters;
- The availability of a wide range of chemical precursors for CVD such as halides, hydrides, and organometallics for the deposition of many materials, including metals, carbides, nitrides, oxides, sulfides, and III–V and II–VI materials.

* Corresponding author.
E-mail address: zaera@ucr.edu (F. Zaera).

1381-1169/$ – see front matter © 2007 Elsevier B.V. All rights reserved.
doi:10.1016/j.molcata.2007.06.010

There are, however, a number of potential problems associated with the design of new CVD processes. In particular:

- Not all CVD reactions are conformal; gas-phase reactions sometimes interfere with the kinetics of the overall film deposition process.
- It is sometimes difficult to control the thickness and morphology of the growing layers: nucleation and three-dimensional island formation, for example, may result in the buildup of rough and discontinuous films.
- Some CVD processes require temperatures above those tolerable in microelectronics fabrication.

Fortunately, it has been recently shown that many of these difficulties can be overcome, or at least minimized, by using a variation of CVD known as atomic layer deposition (ALD). ALD is a chemical deposition method in which two complementary self-limiting reactions are used sequentially and in alternating fashion to slowly build up solid films one monolayer at the time (Fig. 1) [26–29]. ALD was in fact developed in the late 1970s under the name of atomic layer epitaxy (ALE) for the manufacturing of flat-panel displays [30] and later for the preparation of III–V compounds [31–34], but discarded upon the advent of molecular beam epitaxy techniques [35]. It was only in the mid 1990s that ALD regained interest in the silicon-based microelectronics industry for the manufacturing of high aspect-ratio integrated circuits. ALD is presently considered the most promising method for depositing thin, conformal films with atomic-level precision [36]. ALD brings the following advantages to microelectronics manufacturing over conventional CVD methods [28,37]:

- The thickness of films grown by ALD depends only on the number of cycles employed, not on the exposures used in each cycle. This makes its control simple and accurate.
- In ALD there is less of a need for a homogeneous flux of the reactants through the reactor. This makes ALD processes reproducible and easy to scale for large-area coatings without sacrificing conformality.
- ALD offers more flexibility in the design of the operational deposition conditions, requiring lower temperatures than regular CVD.
- There is minimal or no interference from gas-phase reactions during ALD processes because of the separation of the two half reactions in time.
- ALD is easy to use for the manufacturing of layered structures.

On the negative side, ALD, like other CVD processes, suffer from some intrinsic limitations:

- Undesirable contaminants may be deposited within the growing films because of the decomposition of the precursors [38–40].
- Impurities from the carrier gas, such as oxygen or water in the case of oxygen-sensitive TiN or AlN films [41], may be incorporated into the growing films, yielding materials with properties significantly different from those made by PVD [42].
- Films with different microstructure and morphology from those obtained by PVD may develop, especially when post-deposition treatments such as high-temperature annealing are required [43].

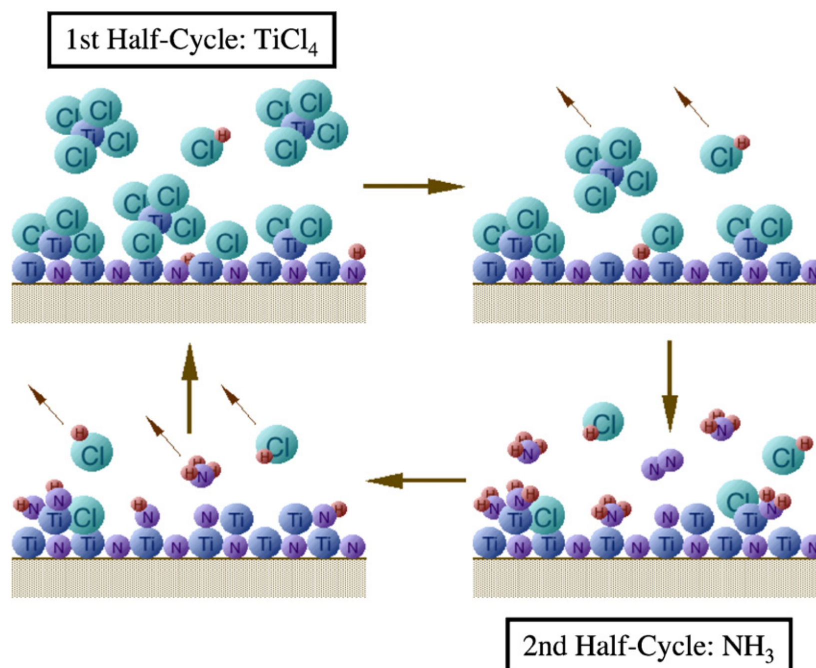

Fig. 1. Schematic representation of the reaction mechanism of atomic layer deposition (ALD) processes, indicating the use of two self-limiting steps involving two different chemicals. Typically, the first provides the metal to be deposited in the form of a volatile inorganic complex, while the second acts as a reducing, oxidizing, displacing, or nitridation agent, helping to remove the undesirable ligands of the first precursor and providing the missing elements for film growth. The example in this figure corresponds to the deposition of TiN films using $TiCl_4$ and NH_3.

- ALD is slow, depositing a fraction of a monolayer in each cycle. This makes it suitable only for the deposition of very thin films [36].

In addition, for an ALD process to work properly, several conditions must be fulfilled [44]:

- The precursors need to be thermally stable and sufficiently volatile for easy transport and to avoid condensation on the substrate, and they should be easy to handle and have low toxicity, explosiveness and flammability. They must also be readily available commercially in high-purity electronic grade and at reasonable cost.
- The surface conversions must be simple, fast, complete, irreversible, self-limiting, and viable at suitable low temperatures.
- The reactions need to be complementary, that is, each must be able to prepare the surface for the other, and to lead to the formation of films with the right stoichiometry.

The resolution of these issues requires a good understanding of the surface chemistry underlying the ALD processes. There is no doubt that atomic layer deposition methods have garnered much attention in recent years, but the emphasis has been on addressing the practical aspects of the implementation of ALD in manufacturing processes with a focus on engineering issues or patentable inventions, not on trying to characterize the fundamental chemistry underpinning these processes. A number of basic chemistry problems that limit the effectiveness of ALD film growth processes have been identified, but those have not been fully addressed to date. We in our group have recently started a program directed to fill this gap between the fast growing pace of the technological developments in ALD and the limitations brought by the poor understanding of the underlying surface chemistry. Below, a brief discussion is provided of some early results from this work on the chemistry of metal nitride deposition.

2. Experimental

Most of the experiments reported here were carried out in a two-chamber stainless steel ultrahigh vacuum (UHV) apparatus briefly described elsewhere [45]. The main volume, evacuated to a base pressure of approximately 1×10^{-9} Torr by using a turbomolecular pump, is equipped with instrumentation for X-ray photoelectron spectroscopy (XPS), mass spectrometry for analysis of the gases, and an ion gun for sample cleaning and depth profiling. The second chamber is also pumped with a separate turbomolecular pump, and can be isolated and pressurized when used as a reactor for the film deposition. A supporting rod is used to hold the solid sample in place and to transfer it between the two chambers. The latter is done by transversing through a set of concentric differentially pumped seals in order to avoid both exposure of the surface to the outside atmosphere and intercontamination between the chambers. The transferring rod can be rotated for better alignment during XPS acquisition, and is capable of cooling down to ~200 K and resistive heating to up to approximately 1000 K. The temperature of the substrate is monitored with a K-type thermocouple inserted into a small hole drilled in the copper hot plate where the substrates are placed, and held in place with a spring made out of tungsten.

The XPS data were collected in the main chamber by using a Leybold EA11 electron-energy analyzer with multichannel detection and a dual Mg Kα ($h\nu = 1253.6$ eV)/Al Kα ($h\nu = 1486.6$ eV) anode X-ray excitation source. Survey spectra were taken by using a constant band-pass energy of 100.8 eV, which corresponds to a spectral resolution of 2.0 eV, and additional high-resolution scans of the regions of interest were obtained using a band-pass energy of 31.5 eV (resolution ~0.9 eV) to accurately determine peak energies and shapes. All the XPS peak positions are reported in binding energies (BE), and were calibrated relative to the reported positions of the substrate peaks and corroborated by the position of the O 1s XPS feature in oxidized samples [46]; they are deemed accurate within ±0.1 eV. The reported spectra were obtained by averaging either 10 or 100 scans, for the survey or high-resolution runs, respectively. XPS peak areas were converted into relative surface atomic concentrations by using reported relative sensitivity factors [46], and checked against reference compounds. Gas dosing during film deposition was carried out in the auxiliary chamber, which was designed to operate as the ALD reactor [47].

The infrared characterization experiments were carried out in a separate system consisting of a transmission infrared cell designed for this type of surface studies [48]. The volume of the reactor is defined by a 0.75 in. thick, 2.75 in. diameter stainless steel spacer sandwiched in between two 2.75 in. flanges holding respective NaCl windows. The spacer has two ports, for the inlet and outlet of gases and for pumping, and feedthroughs for resistive heating of the sample and for the thermocouple wires used to measure temperature. The silica powder was pressed on a $1.0 \times 2.0\,\mathrm{cm}^2$, $30 \times 30\,(\mathrm{lines/cm})^2$, 0.03 mm wire diameter, nickel mesh framed by 1 mm diameter Nichrome wires, which were attached to the grid via spotwelding and mounted via copper barrel connectors to the electrical feedtroughs so that the sample is held in the middle of the reactor volume (Fig. 2). A K-type thermocouple pair was spotwelded to the mesh near the silica powder for temperature measurements. The cell was placed in the sample compartment of a Bruker Equinox 55 infrared spectrometer purged with scrubbed air to eliminate any interfering signals from the water vapor or carbon dioxide in the laboratory's air. IR spectra were taken by averaging 512 scans at 4 cm^{-1} resolution, and normalized by data taken in similar fashion before exposure to any of the ALD gases.

All gases in these experiments, namely, the ammonia (Matheson, anhydrous, 99.99% purity), oxygen (Airgas, ultra high purity), and argon (Airgas, 99.998% purity), were used as supplied, and introduced into the vacuum chamber via leak valves and into the IR cell using regular shut-off valves. The liquids, $TiCl_4$ (Acros, 99.9%), $TaCl_5$ (Alfa Aesar, 99.99%) and $Zr[N(C_2H_5)(CH_3)]_4$ (Sigma–Aldrich, 99.99+%), were purified in situ in our gas-handling manifold by a series of freeze-pump–thaw cycles, and dosed by introducing their vapor into the chamber through the same leak valve used for ammonia dosing.

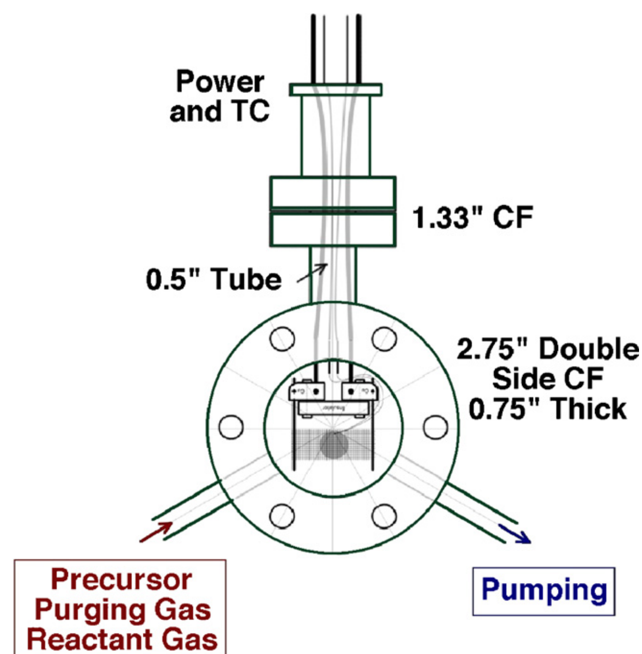

Fig. 2. Schematic representation of the transmission infrared cell used for the characterization of ALD processes on silica. Shown is a frontal view of the 2.75 in. diameter spacer used as the reactor, with the inlet and outlet ports at the bottom for gas flowing and the feedthroughs at the top for sample resistive heating and temperature measurements. The sample, a silica powder, is pressed onto a nickel mesh framed by Nichrome wires and mounted on the electrical feedthroughs so it stands in the middle of the spacer volume and in between the front and back NaCl windows. The whole assembly is placed in the sample compartment of a Bruker Equinox 55 Fourier-transform infrared spectrometer.

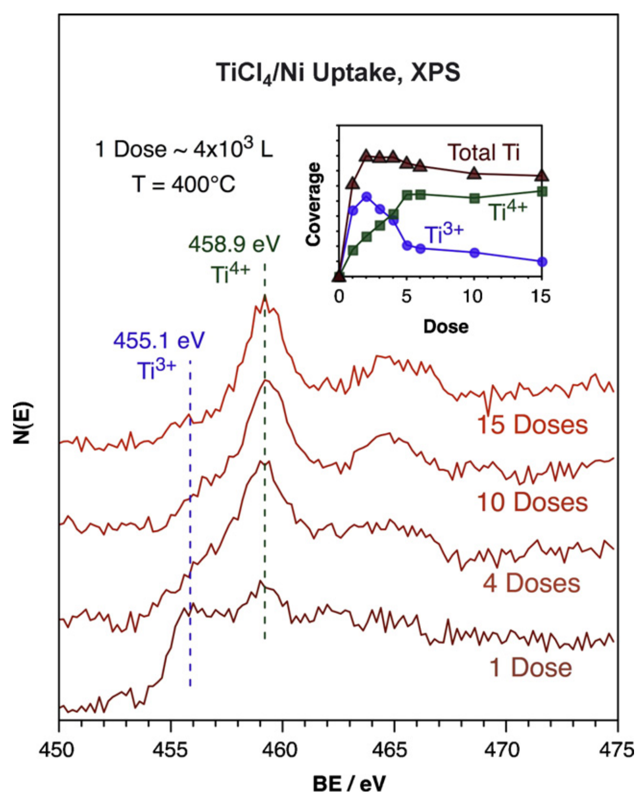

Fig. 3. (Main frame) Ti 2p X-ray photoelectron spectra (XPS) for the uptake of $TiCl_4$ on a nickel foil at 400 °C. The reactant was dosed in pulses of approximately 4×10^3 L. (Inset) Surface concentrations of Ti^{3+}, Ti^{4+} and total Ti as a function of dose, in arbitrary units, estimated from the XPS data. Three key observations derive from these data: (1) the reaction is self limiting, saturating after the first few pulses; (2) the initial titanium is deposited in the form of Ti^{3+}, but is converted at least in part to Ti^{4+} at saturation and (3) the final average stoichiometry of the adsorbates species is $TiCl_{3.5}$.

Most of the XPS experiments were performed using a ∼1 cm^2 nickel foil (Sigma–Aldrich, 0.25 mm thick, 99.995% purity), except those reported in Fig. 5, which were done on a ∼1 cm^2 tungsten foil (ESPI, 0.25 mm thick, >99.98% purity). These surfaces were cleaned by extensive argon sputtering, and checked by XPS before use; most contaminants, including adventitious carbon, could be removed by this treatment, but small amounts of oxygen were often unavoidable. The infrared experiments were performed on a pellet made out of a high surface area silica powder (Degussa Aerosol 200) pressed onto the supporting mesh of the IR cell, as described above. The powder was degassed by extensive heating to 400 °C before use to minimize the amount of adsorbed water in the sample. The elimination of the water was evaluated by IR spectroscopy.

3. Results and discussion

3.1. *TiN from $TiCl_4$ and ammonia*

The case of the growth of TiN films from $TiCl_4$ and NH_3 (Fig. 1) is perhaps the best ALD process studied to date [38,49–57], but many questions remain. For instance, it is not yet clear what the stoichiometry of the resulting films is, how the reduction of the titanium atoms (from Ti^{4+} in $TiCl_4$ to Ti^{3+} in TiN) occurs, or what the oxidation byproduct is. Moreover, although TiN films grown by ALD usually contain oxygen and other contaminants, it has also not yet been clearly established what the sources of those contaminants are, or how they get incorporated into the film. Our surface-science studies have been directed to answer these and other questions about the fundamental chemistry associated with this ALD process.

The chemistry of each individual reaction of the $TiCl_4 + NH_3$ ALD cycle (Fig. 1) was characterized first [47]. Fig. 3 displays representative Ti 2p XPS data obtained during the initial uptake of $TiCl_4$ on a nickel foil at 400 °C. Traces are displayed for the surface obtained after selected $TiCl_4$ doses, each of which consisted of pulses of approximately $(4 \pm 1) \times 10^3$ L. Although most traces are dominated by a Ti $2p_{3/2}$ XPS peak at 458.9 eV typical of Ti^{4+} species [46], the data corresponding to the initial doses display a prominent feature at 455.1 eV more characteristic of Ti^{3+}. This indicates an initial reduction of the $TiCl_4$, at least on metal surfaces, and strongly suggests dissociative adsorption and formation of $TiCl_3$(ads) species.

The uptake of titanium was estimated by integration of the respective Ti 2p XPS signals, and plotted versus number of pulses in the inset. Those results highlight the self-limiting nature of the adsorption: surface Ti (and Cl) saturation is reached after only a couple of pulses. The data also point to the initial predominance of Ti^{3+} species, most of which are reoxidized to Ti^{4+} towards the end of the uptake. Additional measurements from the Cl 2p XPS traces indicate a surface composition at

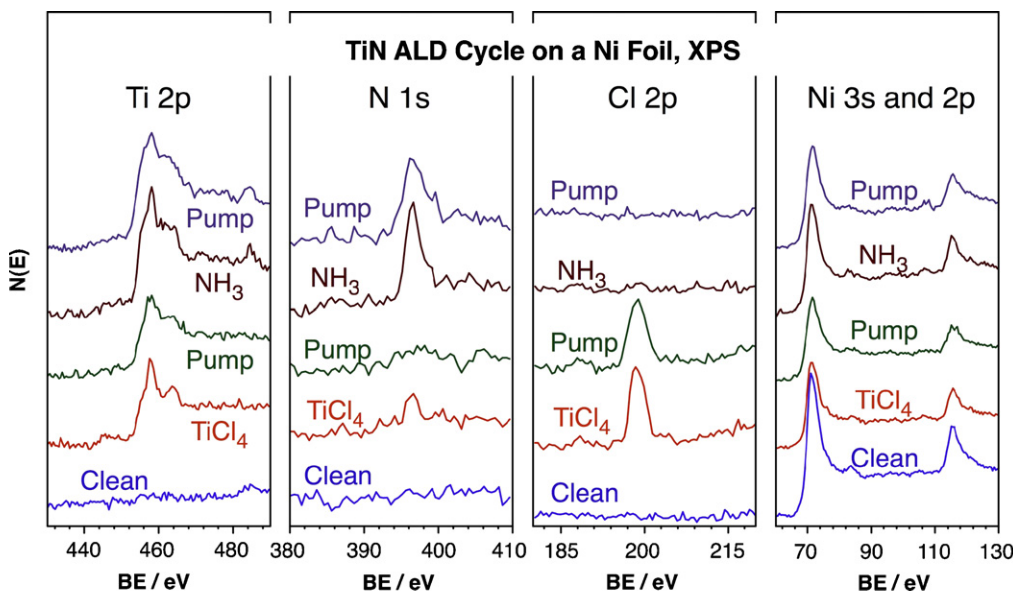

Fig. 4. XPS data for the deposition of TiN films after each of the steps in the ALD cycle indicated in Fig. 1. The results corroborate some of the expected behavior, namely: (1) the incorporation of Ti and N on the surface after $TiCl_4$ and NH_3 treatments, respectively; (2) the removal of most of the chlorine upon ammonia treatment and (3) the attenuation of the XPS signals from the Ni substrate by the TiN deposited film. On the other hand, they also point to some unexpected behavior: (1) the average stoichiometry of the surface species after the first half of the cycle amounts to only about $TiCl_{3.5}$; (2) some of the Ti atoms are reduced to a Ti^{3+} state during this initial uptake, and (3) the final film is not stoichiometric but rich in nitrogen.

saturation of approximately Cl/Ti ~ 3.5, once again suggesting partial reduction and some chlorine elimination. Evidence for $TiCl_4$ dissociative adsorption has been previously reported on W(1 0 0) [58] and W(1 1 0) [59], and also on Si(1 0 0) [60], but disproportionation such as that seen here has not, to the best of our knowledge, being discussed before.

Subsequent treatments of this $TiCl_x$ layer with ammonia lead to titanium nitride formation. This is clear from the XPS data in Fig. 4, which correspond to the sequence of steps that constitute one cycle in the ALD process. The expected behavior is corroborated by these data, namely: (1) the initial exposure of the clean nickel foil to $TiCl_4$ results in the growth of XPS peaks for both titanium (BE(Ti 2p) ~ 458 eV) and chlorine (BE(Cl 2p) ~ 198 eV); (2) both peaks survive pumping in vacuum but change upon ammonia treatment, at which point the chlorine peak is replaced by a new feature for N (BE(N 1s) ~ 397 eV) and (3) a submonolayer quantity of titanium nitride is deposited and remains on the surface after further pumping, at the end of the ALD cycle.

Thick titanium nitride films can be grown by repetition of the ALD cycles described above. Results from quantitation of the appropriate XPS data as a function of the number of ALD cycles are summarized in Fig. 5 in the form of average atomic surface compositions and N/Ti atomic ratios. An exponential decay of the XPS signal for the substrate (tungsten in this case) as a function of the number of deposition cycles is accompanied by exponential growths of the signals for titanium and nitrogen, indicating a constant deposition rate (estimated at approximately 0.04 nm/cycle [47]). Moreover, although the stoichiometry of the film varies slightly during the ALD growth, it always remains rich in nitrogen (N/Ti ~ 1.2–1.4). It should also be pointed out that there is always a fixed amount of Ti^{4+} in these films, as indicated by the Ti 2p XPS signal detected at 457.6 eV binding energy (data not shown) [47]. Additional depth profiling data, obtained via argon sputtering, show that the N/Ti ratio decreases significantly and reaches a constant value of N/Ti ~0.9 ± 0.1 after removal of the topmost layer, before 3 min of sputtering (Fig. 5, right side). Given that this is accompanied by the selective removal of the Ti^{4+} species [47], it is concluded that a thin film of Ti_3N_4 composition always sits on top of the growing TiN film. The Ti_3N_4 top layer is estimated to be about 0.2–0.3 nm thick at all times during the film growth.

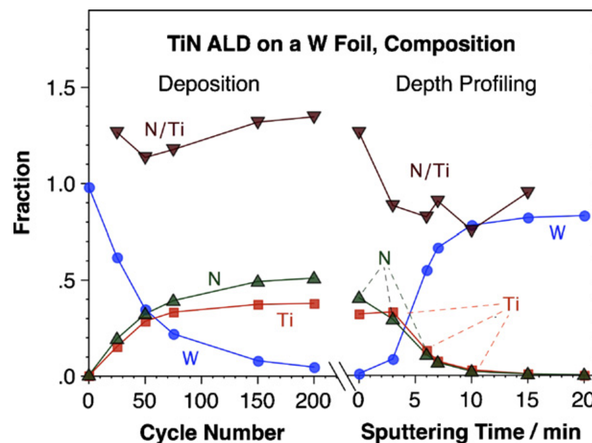

Fig. 5. Summary of the XPS data obtained for the deposition of a titanium nitride film by ALD, in the form of the W (the substrate), N and Ti average atomic concentrations and the N/Ti atomic ratio as a function of cycle number during deposition (left) and of sputtering time afterwards (right). N/Ti ratios higher than unity were always observed during growth but not after light sputtering, indicating the formation of a thin Ti_3N_4 layer on top of the growing TiN film.

3.2. TaN from $TaCl_5$ and ammonia

The generality of the previous conclusion was checked next. For that, the surface chemistry of ALD processes for the deposition of TaN films using $TaCl_5$ and NH_3 was chracterized. TaN films are perhaps some of the most promising for use as diffusion barriers in the microelectronics industry [43,61], because they have reasonably high thermal stability and excellent adhesion to both SiO_2 and copper and do not form any compounds with copper [62–64]. On the negative side, the deposition of TaN needs to be preceded by a previous Ta film-growth step [65], results in only moderately low resistivities [39,40,66,67], requires a strong reducing agent, and is difficult to achieve stoichiometrically. Consequently, the search for an appropriate TaN ALD process is still ongoing [49,68–70].

The issues of reducibility and stoichiometry in TaN ALD echo those identified above in connection with the ALD of titanium nitride. Similar behavior is indeed seen during the growth of tantalum nitride films using $TaCl_5$ and NH_3. Fig. 6 displays representative Ta 4f XPS data to illustrate this point. The bottom four traces, which correspond to the initial uptake of $TaCl_5$ on a nickel foil at 250 °C, show how the first molecules to adsorb on the substrate are reduced to a Ta^{3+} state; notice the main features for the Ta $4f_{7/2}$ and Ta $4f_{5/2}$ photoelectrons at 23.8 and 25.8 eV, respectively. A second pair of XPS peaks does grow at about 26.7 and 28.5 eV after 5 min of exposure to a $TaCl_5$ pressure of $P \sim 1 \times 10^{-5}$ mbar (~2000 L), the binding energies expected for $TaCl_5$ [46]. Subsequent exposure to ammonia (next two traces in Fig. 6) shifts most of the $TaCl_5$ XPS signal to the Ta^{3+} state as the intensity of the N 1s XPS feature also grows and that of Cl 2p XPS peak is almost completely suppressed, all trends expected for TaN formation. Finally, repetition of

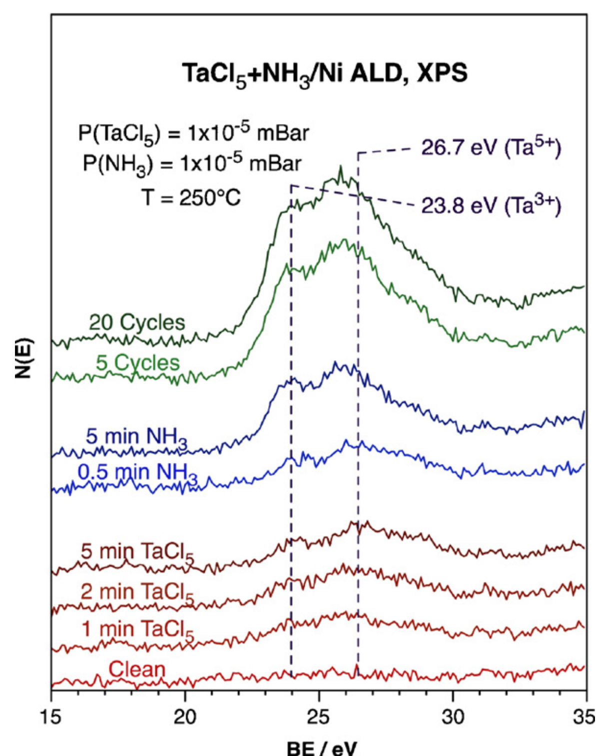

Fig. 6. Ta 4f XPS for the growth of TaN films on a nickel foil at 250 °C using $TaCl_5$ and ammonia. The reactants were dosed using pressures of approximately 1×10^{-5} mbar. The bottom four traces correspond to the initial uptake of $TaCl_5$ and point to the partial reduction of the metal to Ta^{3+} upon adsorption, as in the TiN case. Further exposure to ammonia (next two traces) drives the reduction further, presumably because of the formation of the TaN film. The top two traces show how thicker films can be grown by repeating this cycle. The final average stoichiometry of that film is approximately TaN, but an oxide species is also manifested by additional Ta 4f XPS intensity around 25.8 eV.

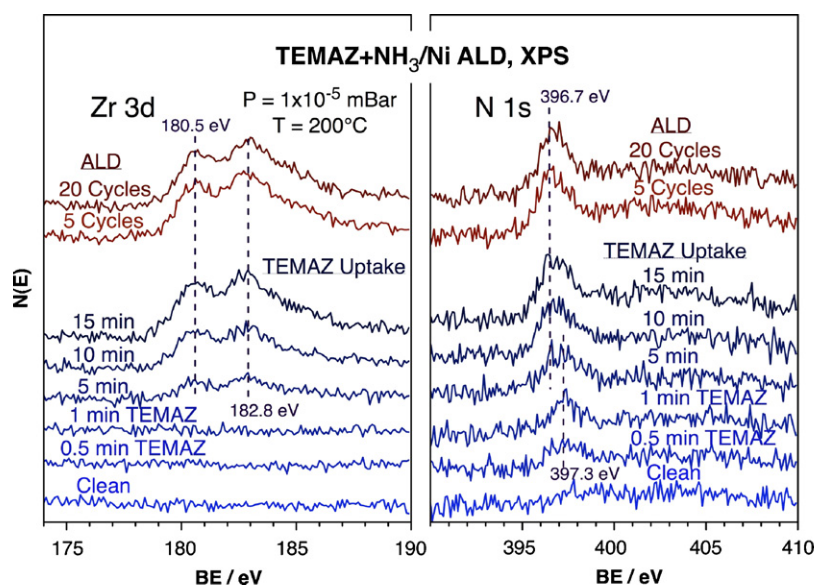

Fig. 7. Zr 3d (left) and N 1s (right) XPS obtained during the growth of a ZrN film on a nickel foil at 200 °C using $Zr[N(C_2H_5)(CH_3)]_4$ (TEMAZ) and ammonia. The reactants were dosed using pressures of approximately 1×10^{-5} mbar. The bottom five traces correspond to the initial TEMAZ uptake, which appears to occur with almost complete reduction to Zr^{3+}. An induction period is also evident during the adsorption, with no zirconium being deposited in the first minute of dosing and only an amine surface species being detected by XPS. Further conversion is clear at higher exposures, at which point the zirconium coverage grows as the N 1s XPS peak shifts to values typical of metal nitrides. The top two traces show the data for the films grown by repeating the TEMAZ + NH_3 cycles, for 5 and 20 cycles, respectively.

this cycle leads to the slow growth of a TaN film (top two traces).

Another issue the ALD of TaN shares with that of TiN is that of the incorporation of impurities in the film, in particular the codeposition of a metal oxide [47]. In this case the problem is evidenced by the excess intensity in the Ta 4f XPS signal at 26.7 eV beyond what is expected for the Ta $4f_{5/2}$ component from the Ta^{3+} species, and also by the O 1s XPS feature seen at approximately 531.8 eV (data not shown). The stoichiometry of this oxide estimated from the areas of the 26.7 eV Ta $4f_{7/2}$ and 531.8 eV O 1s XPS peaks in the final film is Ta_2O_5, a fact also consistent with the binding energies seen for the two elements. The oxide film appears to develop at the interface between the nickel substrate and the TaN growing film, and it is removed last in subsequent depth profiling experiments by argon sputtering (data not shown).

3.3. ZrN from $Zr[N(C_2H_5)(CH_3)]_4$ and ammonia

Finally, inspired by some promising reports in the literature [71], we have within the last few months initiated some preliminary experiments on the deposition of zirconium nitride using $Zr[N(C_2H_5)(CH_3)]_4$ (tetraethylmethylamine-zirconium or TEMAZ). ZrN films have lower resistivity, lead to less void formation in the copper, and are cheaper that TaN [72–75]. In addition, in order to avoid the perceived difficulty in activating metal halides, a number of alternative nitrogen-containing organometallic complexes have been identified for the deposition of nitrides of Ta, Hf and Zr [71,76–78]. However, this ALD is poorly understood, and its viability still in question.

Fig. 7 reports Zr 3d (left panel) and N 1s (right panel) XPS data obtained for the deposition of ZrN films on a nickel foil at 200 °C using TEMAZ and ammonia. Like in the other systems reported above, a reduction of the Zr metal upon adsorption is observed here too. In this case this is identified by the detection of an initial Zr $3d_{5/2}$ XPS peak centered at 180.5 eV, which corresponds to a Zr^{3+} oxidation state [46]. An additional observation derives from the XPS data in this case, though, and that is that there seems to be an induction period before the deposition of the zirconium starts. Note in particular in the uptake data in Fig. 7 (bottom six traces) that no Zr XPS intensity at all is observed before 5 min of exposure of the substrate to TEMAZ (∼2000 L), and that the peak position of the N 1s XPS signal shifts at that point from 397.3 to 396.7 eV; the latter value is typical of metal nitrides, while the former we assign to an amine surface fragment. Also, an oxide is formed here too, hence the additional XPS intensity in the Zr 3d region around 182.8 eV (and the O 1s XPS peak that develops at ∼531.2 eV, data not shown). In this case the oxide appears to block further film growth, since no increase in Zr 3d or N 1s XPS intensity is seen after 20 ALD cycles (Fig. 7, top two traces).

Additional experiments were carried out in a cell capable of in situ infrared surface characterization in order to follow the thermal chemistry of the amine ligands in TEMAZ during the uptake. The initial experiments were performed using

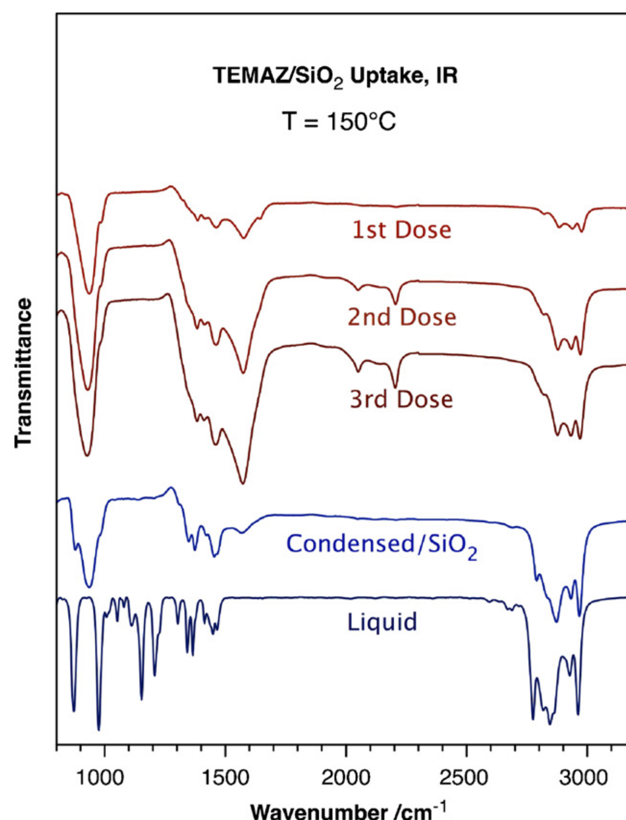

Fig. 8. Transmission infrared spectra obtained for the uptake of TEMAZ on a high surface area silica substrate at 150 °C. The top three spectra correspond to the first three TEMAZ doses (150 mbar in a flow of nitrogen for 60 s) after 1 h of pumping in vacuum (each time) to remove any material condensed within the pores of the solid. The bottom two traces are reference spectra for the liquid and condensed reactant. The deposition of surface species is evidenced by the large peaks at ∼900, 1600 and 2000–2200 cm^{-1} assignable to single, double and triple carbon–nitrogen bonds, respectively, and also by the C–H stretching peaks in the 2700–3000 cm^{-1} region, some of which match those of molecular TEMAZ.

a high surface area silica powder to maximize the IR signal, but results similar to those reported below have been obtained more recently on a silicon wafer (data not shown). The infrared spectroscopy data obtained so far, exemplified by the traces shown in Fig. 8, are quite rich in information, and point to partial decomposition upon adsorption. Most of the peaks around 2700–3000 cm^{-1} due to C–H stretching vibrational modes are preserved, but large new peaks around ∼900, 1600 and 2000–2200 cm^{-1} due to single, double, and triple carbon–nitrogen bonds, respectively, are also seen in the spectra (a detailed peak assignment is provided in Table 1). The modes for the N–CH_3 moiety seem to be all gone, suggesting preferential conversion at that position, but both nitrile and isonitrile species appear to form, which means that some amine groups may detach from the Zr center before dehydrogenating. These results also make clear that the surface adsorbates do not reach a full monolayer coverage even after three cycles. The process is hampered in this case by condensation within the pores of the support, a problem that may be resolved by using higher deposition temperatures. In fact, our experiments showed that temperatures higher than those used here (150 °C)

Table 1
Vibrational assignment of the infrared spectra obtained for TEMAZ both in the liquid phase and adsorbed on a silica powder[a]

Assignment[b]	Liquid	On SiO_2
$\upsilon_{as}(CH_3)$	2961	2967
$\upsilon_{as}(CH_2)$	2928	2931
$\upsilon_{s}(CH_3)$	2863	2873
$\upsilon_{s}(CH_2)$	2843	
$\upsilon_{s}(NCH_2)$	2813	2808
$\upsilon_{s}(NCH_3)$	2776	
$\upsilon(-C\equiv N)$		2203
$\upsilon(-N\equiv C)$		2048
$\upsilon(N{=}C)$		1574
$\gamma(CH_2)$	1468	1459 (br)
$\delta_{as}(CH_3)$	1449	1459 (br)
$\delta_{s}(CCH_3)$	1364	1381
$\delta_{s}(NCH_3)$	1341	
$\upsilon(N-C)$	1225, 1207	
$\upsilon(C-C)$, $\rho(CH_3)$	1153	
$\upsilon(C-C)$, $\rho(CH_3)$	1053	
$\rho(CH_3)$	976, 873	930 (br)

[a] All vibrations are reported in cm^{-1}.
[b] *Abbreviations*: υ, Stretching; γ, scissoring; δ, deformation; ρ, rocking; s, symmetric; as, asymmetric; br, broad.

are indeed needed for the production of nitride films upon subsequent ammonia treatments. Two more observations have derived from these experiments: (1) an induction period is seen for the TEMAZ deposition, the same as in the XPS experiments and (2) thick ZrN films can be grown with TEMAZ alone, presumably by a regular CVD process, as manifested by a golden finish obtain on the powder (and the silicon wafer) after extended exposures.

4. Conclusions

The surface chemistry associated with the atomic layer deposition of metal nitride films was studied by using XPS and infrared spectroscopy. Three precursors were tested in combination with ammonia as the reducing agent, $TiCl_4$, $TaCl_5$ and $Zr[N(C_2H_5)(CH_3)]_4$. Some common features were observed in all three systems. First, the metal center is reduced upon adsorption on the surface, presumably by a disproportionation reaction accompanied by the loss of some of the ligands. Second, ammonia does appear to complete the process by eliminating the remaining chlorine or amine surface species. However, a higher oxidation metal nitride layer appears to always form on top after the ammonia treatment, which may be only reduced after the following dose of the metal complex. Third, the formation of a metal oxide is always detected during the ALD process, apparently at the interface between the substrate and the growing metal nitride film. Finally, metal amines appear to be more reactive than metal chlorides, since they require lower exposures and lower temperatures to work in ALD processes, but they can also deposit metal nitride films by themselves via a regular CVD process. The possible control of the metal amine decomposition so it can be used for film grown in ALD mode is being explored next.

Acknowledgement

Funding for this research was provided by a grant from the US National Science Foundation. Financial assistance for the visit of M. Bouman to UC Riverside was provided by Eindhoven University of Technology.

References

[1] B.W. Wessels, Annu. Rev. Mater. Sci. 25 (1995) 525.
[2] L. Cognolato, J. Phys. IV 5 (1995), C5/975.
[3] R. Gordon, J. Non-Cryst. Solids 218 (1997) 81.
[4] J.J. Coleman, Proc. IEEE 85 (1997) 1715.
[5] L. Niinistö, J. Päiväsaari, J. Niinistö, M. Putkonen, M. Nieminen, Phys. Status Solidi A 201 (2004) 1443.
[6] C.M. Foster, in: R. Ramesh (Ed.), Thin Film Ferroelectric Materials and Devices, Kluwer, Boston, 1997, pp. 167–197.
[7] O. Auciello, C.M. Foster, in: H.S. Nalwa (Ed.), Handbook of Low and High Dielectric Constant Materials and Their Applications, Academic Press, San Diego, 1999, pp. 113–136.
[8] J.S. Kapat, A. Kumar, Mater. Eng. 13 (1999) 441.
[9] T.W. Scharf, S.V. Prasad, T.M. Mayer, R.S. Goeke, M.T. Dugger, J. Mater. Res. 19 (2004) 3443.
[10] C.R. Stoldt, V.M. Bright, J. Phys. D 39 (2006) R163.
[11] R. Thull, D. Grant, in: D.M. Brunette, P. Tengvall, M. Textor, P. Thomsen (Eds.), Titanium in Medicine, Springer, Berlin, 2001, pp. 283–341.
[12] M. Tsapatsis, G.R. Gavalas, G. Xomeritakis, in: N.K. Kanellopoulos (Ed.), Recent Advances in Gas Separation by Microporous Ceramic Membranes, Membrane Science and Technology Series, vol. 6, Elsevier, Amsterdam, 2000, pp. 397–416.
[13] B.A. McCool, W.J. Desisto, Chem. Vapor Dep. 10 (2004) 190.
[14] S. Haukka, E.L. Lakomaa, T. Suntola, in: A. Dàbrowski (Ed.), Adsorption and its Applications in Industry and Environmental Protection, Studies in Surface Science and Catalysis, vol. 120A, Elsevier, Amsterdam, 1999, pp. 715–750.
[15] P. Serp, P. Kalck, R. Feurer, Chem. Rev. 102 (2002) 3085.
[16] A. Gervasini, P. Carniti, J. Keränen, L. Niinistö, A. Auroux, Catal. Today 96 (2004) 187.
[17] M.J. Pellin, P.C. Stair, G. Xiong, J.W. Elam, J. Birrell, L. Curtiss, S.M. George, C.Y. Han, L. Iton, H. Kung, M. Kung, H.H. Wang, Catal. Lett. 102 (2005) 127.
[18] K.F. Jensen, Adv. Chem. Ser. 245 (1995) 297.
[19] J.R. Creighton, P. Ho, in: J.-H. Park, T.S. Sudarshan (Eds.), Chemical Vapor Deposition, Surface Engineering Series, vol. 2, ASM International, Materials Park, 2001, pp. 1–22.
[20] J.E. Crowell, J. Vac. Sci. Technol. A 21 (2003) S88.
[21] S.M. Rossnagel, J. Vac. Sci. Technol. B 16 (1998) 2585.
[22] M. McCoy, Chem. Eng. News 83 (2005) 20.
[23] H.S.P. Wong, D.J. Frank, P.M. Solomon, C.H.J. Wann, J.J. Welser, Proc. IEEE 87 (1999) 537.
[24] M. Schumacher, P.K. Baumann, T. Seidel, Chem. Vapor Dep. 12 (2006) 99.
[25] K.L. Choy, Prog. Mater. Sci. 48 (2003) 57.
[26] S.M. George, A.W. Ott, J.W. Klaus, J. Phys. Chem. 100 (1996) 13121.
[27] B.S. Lim, A. Rahtu, R.G. Gordon, Nat. Mater. 2 (2003) 749.
[28] H. Kim, J. Vac. Sci. Technol. B 21 (2003) 2231.
[29] M. Ritala, in: M. Houssa (Ed.), High-*k* Gate Dielectrics, Institute of Physics, Bristol, Philadelphia, 2004, pp. 17–64.
[30] M. Ahonen, M. Pessa, T. Suntola, Thin Solid Films 65 (1980) 301.
[31] M. Ozeki, Mater. Sci. Rep. 8 (1992) 97.
[32] A. Usui, Proc. IEEE 80 (1992) 1641.
[33] S.M. Bedair, J. Vac. Sci. Technol. B 12 (1994) 179.
[34] T. Suntola, Mater. Sci. Rep. 4 (1989) 261.
[35] Y. Horikoshi, Prog. Cryst. Growth Charact. Mater. 23 (1992) 73.
[36] A. Hand, Semiconductor Int. 26 (2003) 46.
[37] M. Leskelä, M. Ritala, Angew. Chem. Int. Ed. 42 (2003) 5548.

[38] J. Kim, H. Hong, K. Oh, C. Lee, Appl. Surf. Sci. 210 (2003) 231.
[39] Y.Y. Wu, A. Kohn, M. Eizenberg, J. Appl. Phys. 95 (2004) 6167.
[40] O. Van der Straten, Y. Zhu, K. Dunn, E.T. Eisenbraun, A.E. Kaloyeros, J. Mater. Res. 19 (2004) 447.
[41] G. Meng, X. Liu, S. Xie, D. Peng, J. Cryst. Growth 163 (1996) 232.
[42] F. Levy, P. Hones, P.E. Schmid, R. Sanjines, M. Diserens, C. Wiemer, Surf. Coat. Technol. 120–121 (1999) 284.
[43] L. Peters, Semiconductor Int. 26 (2003) 50.
[44] R.G. Gordon, D. Hausmann, E. Kim, J. Shepard, Chem. Vapor Dep. 9 (2003) 73.
[45] K.M. Roth, A.A. Yasseri, Z.M. Liu, R.B. Dabke, V. Malinovskii, K.H. Schweikart, L.H. Yu, H. Tiznado, F. Zaera, J.S. Lindsey, W.G. Kuhr, D.F. Bocian, J. Am. Chem. Soc. 125 (2003) 505.
[46] C.D. Wagner, W.M. Riggs, L.E. Davis, J.F. Moulder, G.E. Muilenberg (Eds.), Handbook of X-ray Photoelectron Spectroscopy, Eden Prairie, Perkin-Elmer Corporation, 1978.
[47] H. Tiznado, F. Zaera, J. Phys. Chem. B 110 (2006) 13491.
[48] F. Zaera, Int. Rev. Phys. Chem. 21 (2002) 433.
[49] L. Hiltunen, M. Leskelä, M. Makelä, L. Niinistö, E. Nykänen, P. Soininen, Thin Solid Films 166 (1988) 149.
[50] M. Ritala, M. Leskela, E. Rauhala, P. Haussalo, J. Electrochem. Soc. 142 (1995) 2731.
[51] J.W. Lim, H.S. Park, S.W. Kang, J. Appl. Phys. 88 (2000) 6327.
[52] C.H. Ahn, S.G. Cho, H.J. Lee, K.H. Park, S.H. Jeong, Met. Mater. Int. 7 (2001) 621.
[53] J. Uhm, H. Jeon, Jpn. J. Appl. Phys. Part 1 40 (2001) 4657.
[54] K.E. Elers, V. Saanila, P.J. Soininen, W.M. Li, J.T. Kostamo, S. Haukka, J. Juhanoja, W.F.A. Besling, Chem. Vapor Dep. 8 (2002) 149.
[55] A. Satta, J. Schuhmacher, C.M. Whelan, W. Vandervorst, S.H. Brongersma, G.P. Beyer, K. Maex, A. Vantomme, M.M. Viitanen, H.H. Brongersma, W.F.A. Besling, J. Appl. Phys. 92 (2002) 7641.
[56] S. Smith, W.-M. Li, K.-E. Elers, K. Pfeifer, Microelectron. Eng. 64 (2002) 247.
[57] J. Gelatos, L. Chen, H. Chung, R. Thakur, A. Sinha, Solid State Technol. 46 (2003) 44.
[58] W. Chen, J.T. Roberts, Surf. Sci. 359 (1996) 93.
[59] A. Sandell, M.P. Andersson, A.J. Jaworowski, J.T. Roberts, P. Uvdal, Surf. Sci. 521 (2002) 129.
[60] T. Mitsui, E. Hill, R. Curtis, E. Ganz, J. Vac. Sci. Technol. A 19 (2001) 563.
[61] D. Vogler, P. Doe, Solid State Technol. 46 (2003) 35.
[62] K. Holloway, P.M. Fryer, C. Cabral Jr., J.M.E. Harper, P.J. Bailey, K.H. Kelleher, J. Appl. Phys. 71 (1992) 5433.
[63] M.A. Nicolet, Appl. Surf. Sci. 91 (1995) 269.
[64] J.-C. Lin, C. Lee, J. Electrochem. Soc. 146 (1999) 3466.
[65] I. Goswami, R. Laxman, Semiconductor Int. 27 (2004) 49.
[66] S.M. Rossnagel, A. Sherman, F. Turner, J. Vac. Sci. Technol. B 18 (2000) 2016.
[67] P. Singer, Semiconductor Int. 27 (2004) 40.
[68] M. Ritala, P. Kalsi, D. Riihela, K. Kukli, M. Leskela, J. Jokinen, Chem. Mater. 11 (1999) 1712.
[69] M. Juppo, P. Alen, M. Ritala, M. Leskela, Chem. Vapor Dep. 7 (2001) 211.
[70] P. Alen, M. Juppo, M. Ritala, M. Leskela, T. Sajavaara, J. Keinonen, J. Mater. Res. 17 (2002) 107.
[71] J.S. Becker, E. Kim, R.G. Gordon, Chem. Mater. 16 (2004) 3497.
[72] M. Östling, S. Nygren, C.S. Petersson, H. Norström, R. Buchta, H.-O. Blom, S. Berg, Thin Solid Films 145 (1986) 81.
[73] H. Yanagisawa, K. Sasaki, H. Miyake, Y. Abe, Jpn. J. Appl. Phys. Part 1 39 (2000) 5987.
[74] M.B. Takeyama, A. Noya, K. Sakanishi, J. Vac. Sci. Technol. B 18 (2000) 1333.
[75] C.-S. Chen, C.-P. Liu, H.-G. Yang, C.Y.A. Tsao, J. Vac. Sci. Technol. B 22 (2004) 1075.
[76] D.M. Hoffman, Polyhedron 13 (1994) 1169.
[77] C.H. Winter, Aldrichim. Acta 33 (2000) 3.
[78] A. Baunemann, Y. Kim, M. Winter, R.A. Fischer, Dalton Trans. (2006) 121.